PAPER NAME

2021_The Crystal Structure Analysis of Silver Nanowires Using Rietveld Method for Optoelectronic App

AUTHOR

Junaidi Junaidi

WORD COUNT

5658 Words

CHARACTER COUNT

27211 Characters

PAGE COUNT

12 Pages

FILE SIZE

5.3MB

SUBMISSION DATE

Jun 29, 2022 10:33 AM GMT+7

REPORT DATE

Jun 29, 2022 10:34 AM GMT+7

17% Overall Similarity

The combined total of all matches, including overlapping sources, for each database.

- 15% Internet database
- 6% Publications database
- Crossref database
- Crossref Posted Content database
- 3% Submitted Works database

Excluded from Similarity Report

- Bibliographic material
- Quoted material
- Cited material
- Small Matches (Less then 10 words)
- Manually excluded sources
- Manually excluded text blocks

Journal of Nano Research
ISSN: 1661-9897, Vol. 71, pp 1-12
doi:10.4028/www.scientific.net/JNanoR.71.1

Submitted: 2021-06-28
Revised: 2021-10-07
Accepted: 2021-11-15
Online: 2022-01-25

The Crystal Structure Analysis of Silver Nanowires Using Rietveld Method for Optoelectronic Application

Junaidi[1,2,a*], Lina Afriliani[1,b], Posman Manurung[1,c], Simon Sembiring[1,d], Kuwat Triyana[3,e] and Sutopo Hadi[4,f]

[1]Department of Physics, Faculty of Mathematics and Natural Sciences, Universitas Lampung, Bandar Lampung, Indonesia 35145

[2]Intrumentations Research Group, Department of Physics, Universitas Lampung, Bandar Lampung, Indonesia 35145

[3]Departement of Physics, Universitas Gadjah Mada, Yogyakarta, Indonesia 55281

[4]Department of Chemistry, Faculty of Mathematics and Natural Sciences, Universitas Lampung, Bandar Lampung, Indonesia 35145

[a]junaidi.1982@fmipa.unila.ac.id, [b]lina.afriliani1503@student.unila.ac.id, [c]posman.manurung@fmipa.unila.ac.id, [d]simon.sembiring@fmipa.unila.ac.id, [e]triyana@ugm.ac.id, [f]sutopo.hadi@fmipa.unila.ac.id

Keywords: silver nanowires, crystal structure, Ethylene Glycol, Propylene Glycol, XRD, TEM

Abstract. In this study, the synthesis and analysis of the crystal structure of silver nanowires (AgNWs) have been performed using the polyol method. In this research, materials used as the main raw material were silver nitrate ($AgNO_3$). Polyvinyl pyrrolidone (PVP) was used as a capping agent and stabilizer, and Iron (III) Chloride ($FeCl_3$) for controlling the shape and size of AgNWs. AgNWs were synthesized using two different solvents i.e., ethylene glycol (EG) and propylene glycol (PG). The crystal structure of AgNWs was analyzed using X-ray diffraction (XRD) with a scanning 2θ in the range of 20° to 90°. Furthermore, the structure and electron diffraction patterns were analyzed using transmission electron microscopy (TEM). The XRD pattern of the AgNW sample also has five diffraction peaks, these five diffraction peaks were identified at 38.24°, 44.42°, 64.54°, 77.52°, and 81.68° representing lattice constants (111), (200), (220), (311), and (222), respectively. Based on the results of the calculation of lattice constant values of AgNWs-EG and AgNWs-PG were 4.084 Å. The TEM images of AgNWs-EG have a diameter of 84 to 133 nm, corresponding to the SEM calculation data having a diameter of 109 ± 22 nm. AgNWs-PG has a diameter of 84 to 264 nm. The study results revealed that the results of the characterization performed are interconnected. The XRD characterization results revealed that both samples were crystal-indexed. AgNWs-PG has a larger crystal size than AgNWs-EG.

Introduction

Research on nanomaterials, such as nanowires (NWs), is particularly important in the last few decades [1-3]. Nanowires are 1D nanostructured materials with diameters between 10 and 200 nm and lengths between 5 and 100 μm [4-8]. The synthesis of NWs continues to be of interest to researchers and the development of materials for the synthesis of NWs from various types of metals. In terms of metal types, research was conducted on NWs, such as copper (Cu), gold (Au), platinum (Pt), iron (Fe), and silver (Ag). Ag metals are more widely used for NW synthesis than other metals because Ag is less susceptible to oxidation while it is readily available but cheaper [8]. Ag metal in the form of silver nitrate ($AgNO_3$) is easily formed into nanocrystals or nanostructures, such as silver nanoparticles (AgNPs), silver nanorods (AgNRs), and silver nanowires (AgNWs) [9-11].

In the synthesis of AgNWs, the main concern is still the development of the types of capping agents and solvents. For the development of such agents, NW synthesis has been attempted using polyvinylpyrrolidone (PVP) and polyvinyl alcohol (PVA) [10, 12]. Various types of solvents in the synthesis of NWs have been developed, including Ethylene Glycol (EG), glycerol, deionized (DI)

water, and Propylene Glycol (PG). EG is a solvent that can decompose into glycolaldehyde and water, and it plays a role in reducing Ag^+ to Ag atom. Ethylene glycol has a boiling point of 197°C, and it is an approach to the melting point of $AgNO_3$ about 209°C; therefore, EG as a solvent can produce AgNWs with a high aspect ratio. The chemical properties of EG are easily oxidized to form aldehydes and carboxylic acids by oxygen, nitric acid, and other oxidizing agents. Varying reaction conditions can affect the formation of the desired oxidation product. Another type of solvent is glycerol that plays a significant role in regulating nucleation in the initial reaction. The high viscosity of glycerol can slow down the rate of change of Ag^+ to Ag atom; thus, the resulting AgNWs become uniform. However, one disadvantage of glycerol is its high cost due to its extensive and diverse use [13]. In addition to the two solvents above, synthesis of NWs by using DI water has been attempted. The use of deionized water is a cheap and easy way to obtain solvent. However, DI water synthesis is difficult, and the obtained AgNWs tend to have a low aspect ratio [14]. PG has a boiling point approach to silver metal, which is 188°C. PG has water-soluble, acetone, and chloroform properties. But until now, only a few researchers use PG for the synthesis of AgNWs, even though it has a high potential in the synthesis of AgNWs with high aspect ratio [9]. PG is colorless, thick, and odorless and has a sweet taste and good stability at a pH of 3–6 [15]. PG is more widely used as a solvent and preservative in various parental and nonparental formulations. It has a relatively low price compared with other solvents for the synthesis of AgNWs [16].

So far, there has been no analysis of the crystal properties of AgNWs. The discussion regarding crystal structure is only limited to the diffraction peak values resulting from the combined XRD and TEM characterization results without any comprehensive explanation. For this reason, in this study, we attempted to synthesize and analyze the crystal structure of AgNWs. Silver nanowires were synthesized using two different solvents, namely, EG and PG, to compare the result of AgNWs. The results of the study are expected to assist researchers in analyzing the diffraction result data from AgNW samples synthesized using the polyol method [10].

The AgNWs are widely applied in manufacturing transparent conductive electrodes (TCEs) for optoelectronics, such as touch screens, transparent heaters, photovoltaics, organic light-emitting diodes (OLEDs), and other electronic devices. The AgNW ink systems can be tailored to meet a particular specification. The benefits of TCE systems include low-cost solution for many applications compared with TCO coatings, reproducible batch-to-batch performance, low-temperature post-processing (<120˚C), high transmission over a broad range of sheet resistance, and compatibility with both flexible and glass substrates [17-19].

Materials and Methods

The materials used for synthesizing of AgNWs through polyol method included silver nitrate ($AgNO_3$, 99%, Merck), polyvinyl pyrrolidone (PVP), Sigma-Aldrich, Mw. 55000 g/mol), ethylene glycol (EG, 99%, Merck), propylene glycol (PG, 99%, Merck), and Iron(III) chloride ($FeCl_3.6H_2O$, Sigma Aldrich), ethanol (EtOH, 98%, Merck). Synthesis of AgNWs using EG and PG as a solvent as shown in Fig. 1.

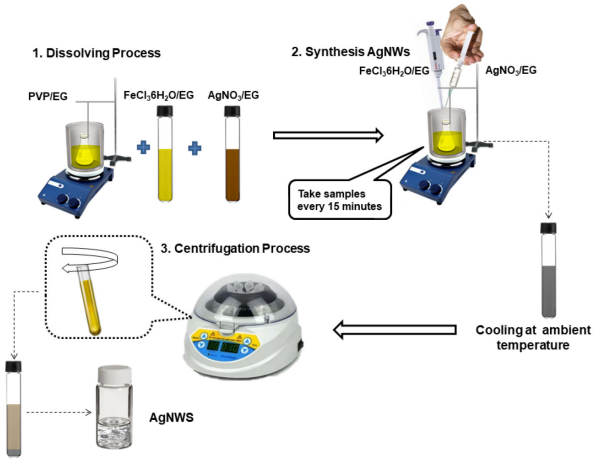

Figure 1. Synthesis of AgNWs using EG/PG by polyol method

From Fig. 1, the synthesis of AgNWs was done by heating the oil bath on the hotplate stirrer to a stable temperature of 130 ºC. Furthermore, as much as 0.45 M PVP in 20 mL EG/PG is heated and distributed at 350 rpm for 1 hour. After 1 hour, an amount of 0.04 M $FeCl_3.6H_2O$ of 100 uL was injected into a PVP solution using a micropipette. Then 0.3 M of $AgNO_3$ as much as 8 ml injected drop by drop using a syringe into the previous solution for about 40 minutes. After that, the solution is rotated for 2 hours until AgNWs formed. Finally, the AgNWs solution was cooled and washed at room temperature for 30 minutes, and then AgNWs were centrifuged at 3000 rpm for 5 minutes using ethanol for three times.

The crystal structure of AgNWs was analyzed using XRD (Shimadzu R6000) by CuKα (λ = 1.54184 Å) with a scanning 2θ in the range of 20° to 90°. Furthermore, the structure and electron diffraction patterns were analyzed using transmission electron microscopy (JEOL, JEM-2010) by accelerating voltage of 120 kV.

Results and Discussion

The crystal structure analysis of AgNWs was conducted using the XRD pattern. This characterization aims to determine the crystal structure formed from AgNW powder. AgNW powder is dried and mashed using oven for approximately 4 h. The XRD pattern of the AgNW samples obtained was then analyzed employing the HighScore Plus application using 2θ parameters, d_{space} (Å), and intensity. Furthermore, the data was matched with the reference database used by the International Center for Diffraction Data (ICDD). The characterization of XRD in AgNWs synthesized using EG (AgNWs-EG) and AgNWs synthesized using PG (AgNWs-PG) is presented in Fig. 2.

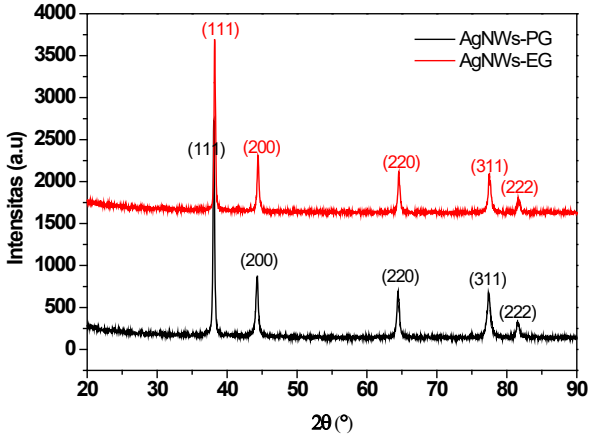

Figure 2. XRD Patterns of AgNWs-EG and AgNWs-PG.

The XRD characterization was conducted to obtain the crystal structure of AgNWs. The unit used for CuKα is in Angstrom (Å) with 20°to 90° with a step of 0.026°. This step is calculated by subtracting the second line and the first line. Figure 2 presents the crystal structure of AgNWs-EG and AgNWs-PG. Figure 2(a) presents the XRD pattern for AgNWs-PG consisting of five diffraction peaks. All peaks were identified as Ag cubic phase with a face-centered cubic (FCC) crystal structure [9]. The XRD pattern shows that the peaks of intensity located at angles 38.10°, 44.29°, 64.43°, 77.41°, and 81.57° are related to the lattice planes (111), (200), (220), (311), and (222) sequentially obtained using the XRD analysis software.

Similar to Fig. 2(a), Fig. 2(b), which presents the XRD pattern of the AgNWs-EG sample, also has five diffraction peaks. The five diffraction peaks were identified at 38.24°, 44.42°, 64.54°, 77.52°, and 81.68°, representing lattice constants (111), (200), (220), (311), and (222), respectively. From the results of the calculation of lattice constant values obtained by 4.084 Å for AgNWs-EG and 4,084 Å for AgNWs-PG. Calculation of lattice constants according to literature a = b = c = 4.086 Å [13]. Digital data from the XRD analysis results are then refined. The refinement process is the fitting technique calculated diffraction data patterns and measured diffraction data patterns with ICDD. The output information contains, among others, a match index of the calculated diffraction pattern with a measured diffraction pattern, as presented in Fig. 3. Reitica refinement results are output information that contains details on crystal structure parameters, such as that presented in Table 1.

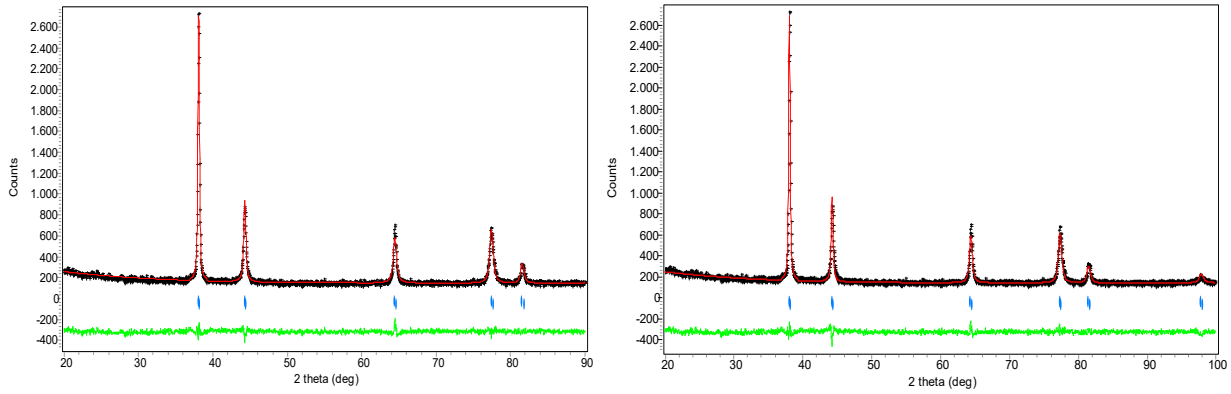

(a) (b)

Figure 3. Refinement results from samples of (a) AgNWs-EG and (b) AgNWs-PG.

Table 1. Information on the results of the refinement

Parameters	ICDD	Sample	
		AgNWs-PG	AgNWs-EG
χ^2	-	1.16	1.25
R_{wp} (%)	-	8.65	8.37
R_p (%)	-	6.87	6.69
R_{exp} (%)	-	7.25	7.35
R_B (%)	-	0.99	0.67
Lattice constant	-	-	-
a (Å)	4.0861	4.0870	4.0870
b (Å)	4.0861	4.0870	4.0870
c (Å)	4.0861	4.0870	4.0870
Volume of cell (Å^3)	68.22	68.2715	68.2691
Molecular weight	-	430.7900	430.7900
Density (g/cc)	-	10.4730	10.4740

Figure 3 presents the results of the refinement of AgNWs-PG samples (Fig. 3(a)) and AgNWs-EG (Fig. 3(b)). Calculation of the diffraction patterns is indicated by red lines originating from the ICDD. The measured diffraction pattern is indicated by a dashed black line from the X-ray diffraction data (XRD); the green line indicates the difference between the two intensities, whereas the blue line

indicates the position of the corresponding peaks. Peak intensity and position will affect the refinement match index. This matching can be declared complete if the difference between the calculated and measured patterns has relatively small fluctuations that can be observed visually and a good value of fitting (GoF) < 4%).

Table 1 indicates that there was a lot of silver in the sample which is supported with matched results of refinement ($\chi 2$, R_{wp}, R_p, R_B, and R_{exp}). For $\chi 2$ indicates a GoF value that refers to the value of $\chi 2$ produced. The value of $\chi 2$ is obtained from the comparison of R_{wp} and R_{exp} squared. The value of R_p will be smaller if the difference in the intensity of observed and calculated data is also getting smaller. The R_B factor shows the calculated and observed intensity of integration for the Bragg to reflection event. The XRD analysis results can also be used to determine the crystal size of AgNWs by the highest peak analyzed using the OriginLab software. The crystal size can be calculated using Scherer Equation in Eq. 1 obtained by particle size as in Table 2.

$$L = \frac{0.94\lambda}{\beta \cos\theta} \tag{1}$$

where L shows the size of the crystal (nm), θ shows Bragg's angle, λ is the wavelength of X-rays (0.15406 nm) and β shows the FWHM value is the width of the diffraction peak at half the maximum intensity analyzed using OriginLab 9.0 software.

Table 2. Calculation of crystal size from XRD data of AgNWs-PG and AgNWs-EG

Sample	K	2θ (°)	λ (nm)	FWHM (°)	FWHM (radian)	L (nm)
AgNWs-EG	0.94	38.244	0.15406	0.2842	0.00496	30.90
AgNWs-PG	0.94	38.108	0.15406	0.2471	0.00431	35.52

Table 2 presents the FWHM value of the AgNWs-EG sample calculated using the OriginLab software from the peak, which has the highest intensity at an angle of 38.244° for 0.00496 radians, with a crystal size of 30.90 nm, whereas the AgNWs-PG obtained the FWHM value at an angle of 38.108° for 0.00431 radians. Both samples were formed from the XRD results by calculating using the Scherer Equation. From Table 2, it can be seen that AgNWs-PG has a larger crystal size than AgNWs-EG. The FWHM value is used to calculate the size of the crystal; the value is inversely proportional to the size of the crystal, wherein the smaller the FWHM value, the larger the crystal size [18]. The results of these calculations indicate that the size of AgNWs in nm so that AgNWs are nanomaterials. To find out the diameter and shape of the tip of AgNWs-EG was analyzed using TEM, as presented in Fig. 4.

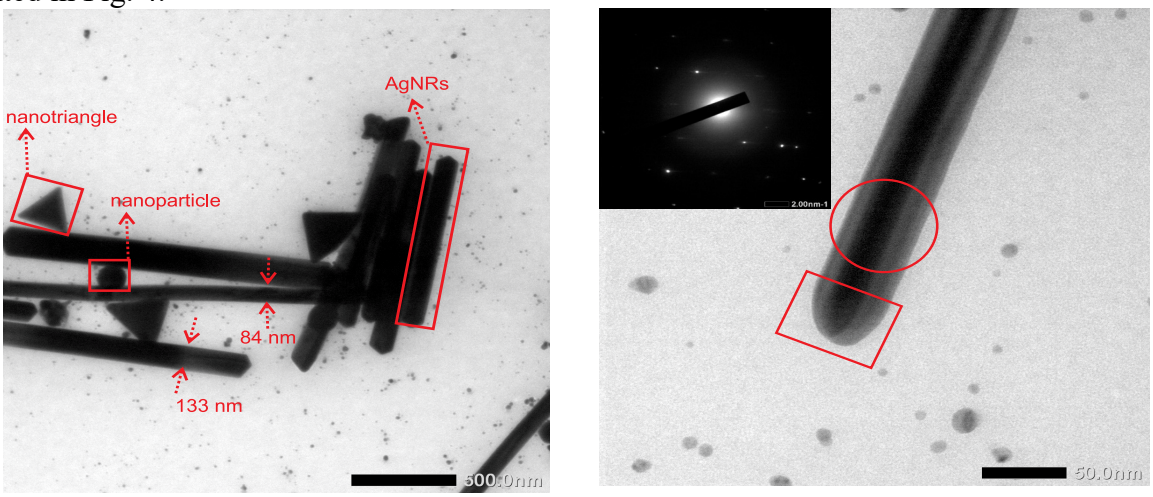

(a) (b)

Figure 4. TEM images from samples (a) AgNWs-EG and (b) tip shape of AgNWs-EG.

Figure 4(a) presents the TEM images of AgNWs-EG that has a diameter of ~84 and ~133 nm, which corresponds to the SEM calculation data having a diameter of 109 ± 22 nm. The results of SEM and TEM characterization of AgNWs showed almost the same values. Figure 4(a) also shows that besides NWs, there are still other particles, such as AgNPs, and nanotriangles formed from a single crystal. The single crystal cannot grow into AgNWs as described; this is influenced by the temperature and reaction time the longer the reaction temperature. The reaction temperature of 130°C for 2 h still many AgNPs, AgNRs, and nanotriangles are formed. If the reaction time is increased it can cause AgNWs that have reached saturation to be broken [21, 22]. Relatively low reaction temperatures do not provide enough energy to activate specific aspects for the growth of AgNWs. In addition, AgNWs-EG still formed many other particles that were found to be less clean at the time of washing. Figure 4(b) shows that the tip of a single NW is decahedral [23]. The growth mechanism in the form of silver seeds is presented in Fig. 5.

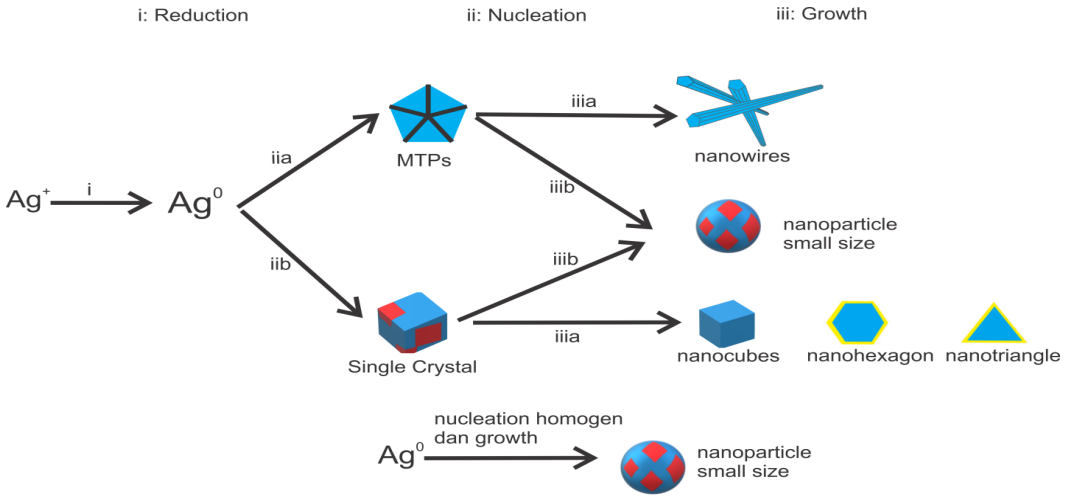

Figure 5. Growth mechanism in the form of silver seeds.

Fig. 5 is the process of AgNWs formation begins with the breakdown of Ag^+ and NO^- ions from $AgNO_3$. The Ag^+ ion then interacts with AgCl to form AgNPs and multi twin particles (MTPs) and undergo an etching process that leads to the formation of AgNPs, AgNRs, AgNWs and other particles. At the nucleation stage AgNWs grow into various forms, this final form depends on the initial seed type before growing into AgNWs and other particles. In the final stage, there is an interaction between the surface of Ag with the capping agent that forms a strong Ag-O bond. MTPs seed with a pentagonal shape that will grow into AgNWs while other seeds from single crystals form AgNPs, nano hexagons, nano triangles and nanocubes. As a result of strong Ag-O bonding, the seeds of MTPs undergo an elongation process leading to the formation of AgNWs. The SAD pattern of diffraction indexed of AgNWs-EG as shown in Fig. 6.

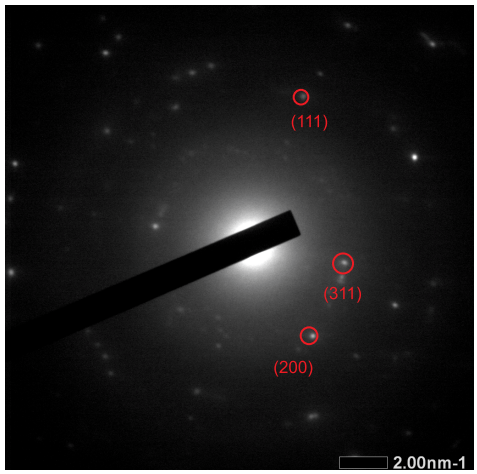

Figure 6. SAD pattern of diffraction indexed of AgNWs-EG.

Parts of the single AgNWs were then analyzed using the selected area diffraction (SAD) pattern (Fig. 6) to prove the diffraction pattern and the d_{hkl} values formed which were matched with ICCD No. 03-065-2871. The lattice constant value obtained from the calculation of 4.082 Å is in accordance with the theory of lattice constant value owned by Ag of 4.082 Å [9].

After manually indexing, crystal diffraction indexed SAD pattern is obtained as shown in Fig. 6. The results of manually calculating the SAD diffraction pattern parameters are shown in Table 3.

Table 3. Manually analyzing SAD AgNWs-EG pattern parameters

No	d_{space} (Å)	d_{ICDD} (Å)
1	1.2353	1.2320
2	2.0479	2.0430
3	0.9110	0.9137
4	2.3118	2.3591

Table 3 shows that the d_{space} parameter (obtained from the manual analysis of the SAD pattern) does not fully correspond to the d parameter (obtained from the ICDD); there is a slight difference from the two d data. However, all the d_{space} values are in the range of the ICDD values. Table 3 shows that the particle diffraction pattern is an FCC structured crystal field and the values are in compliance with the ICDD that the AgNWs structure is FCC with a field index as displayed in Fig. 6. After obtaining the dspace value in Table 3, manual calculation is performed using Microsoft Excel to prove that the dspace value corresponds to the hkl value formed in the XRD results using Eq. 2 and a lattice constant in the theory of 4.082 Å, with the results presented in Table 4 [9].

$$\frac{1}{d_{hkl}^2} = \frac{h^2 + k^2 + l^2}{\alpha^2} \tag{2}$$

Table 4. Analysis of the SAD pattern values of the AgNWs-EG

d_{space} (Å)	h	k	l	d_{space} theory	α	$\sqrt{h^2 + k^2 + l^2}$
1.2353	1	0	0	4.0861	4.082	1
2.0479	0	1	0	4.0861	4.082	1
0.9110	0	0	1	4.0861	4.082	1
2.0479	2	0	0	2.0410	4.082	2
2.0479	0	2	0	2.0410	4.082	2
2.0479	0	0	2	2.0410	4.082	2
0.9110	2	2	2	1.1784	4.082	3.4641
2.3118	1	1	1	2.3568	4.082	1.7320
1.2353	3	1	1	1.2319	4.082	3.3166
1.2353	1	3	1	1.2319	4.082	3.3166
1.2353	1	1	3	1.2319	4.082	3.3166
0.9110	4	2	0	0.9137	4.082	4.4721
2.0479	4	2	2	0.8342	4.082	4.8989
1.1769	4	4	4	0.5897	4.082	6.9282

Table 4 shows that the *hkl* values were analyzed manually using Eq. 2 which aims to match the d_{space} values of the research data with the d_{space} of the theory. In this case, to determine the suitability of the d_{hkl} value. The value of the traffic is entered randomly. However, Table 5 shows the corresponding plane fields (111), (311), (420) and (200) because the crystal structure formed is FCC so that the value of the *hkl* has the characteristics of all even or odd. In addition, the d_{space} calculation value is still in the theoretical d_{space} range even though the values are not the same, so it indicates that

the *hkl* fields that are formed correspond. While the other fields of *hkl* don't correspond to the d_{space} value because the resulting values are not the same and are spaced far enough. The results of the TEM analysis on the AgNWs-PG sample are shown in Fig. 7.

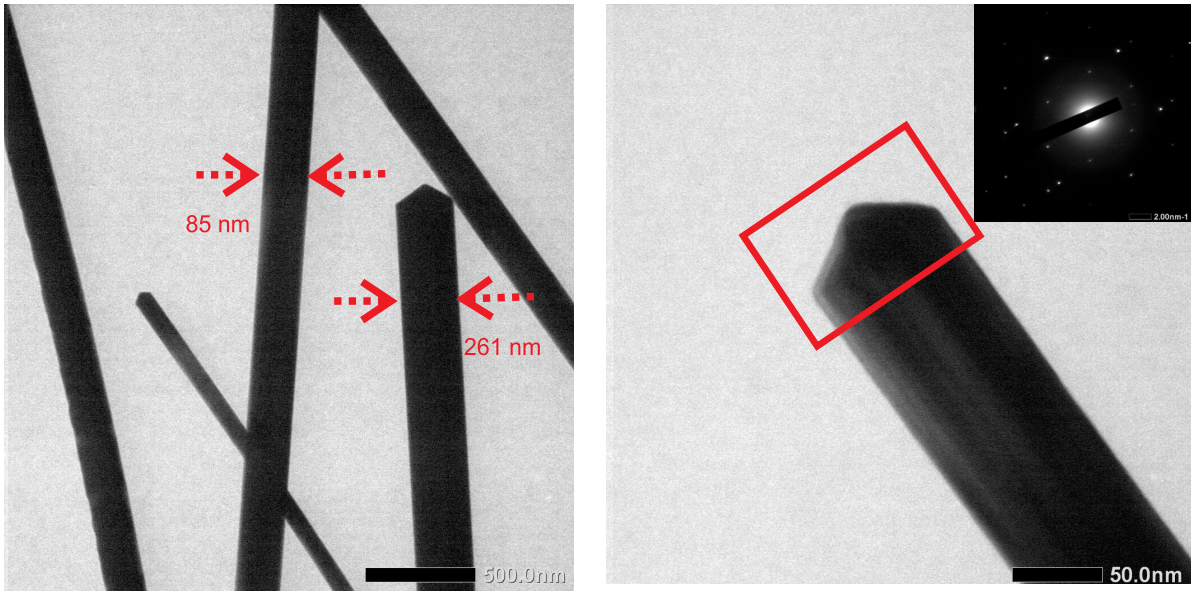

(a) (b)

Figure 7. TEM images of (a) AgNWs-PG and (b) tip shape of AgNWs-PG

Fig. 7(a) shows that AgNWs-PG has a diameter of ~84 nm and ~264 nm. From the morphology of AgNWs-PG analyzed using TEM, the results are that the diameter of the TEM is corresponding or is in the SEM data range results. The AgNWs-PG sample from the picture shows that no other particles have formed besides NWs. Fig. 7(b) shows the shape of the tip of the formed NWs is decahedral. The TEM results show that the AgNWs sample has a larger diameter than the AgNWs-EG sample. The SAD pattern of the AgNWs-PG sample is shown in Fig. 8.

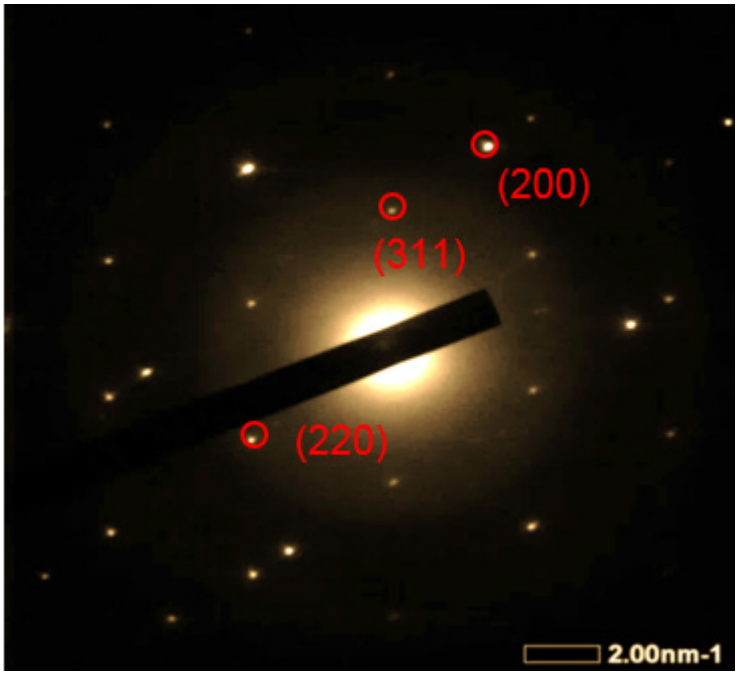

Figure 8. SAD Patterns of AgNWs-PG

After manually indexing, crystal diffraction indexed SAD pattern image is obtained as shown in Fig. 8. The results of the manual calculation of the SAD diffraction pattern parameters are shown in Table 5.

Table 5. Manually analyzing SAD pattern parameters of AgNWs-PG

No	d_{space} (Å)	d_{ICDD} (Å)
1	1.2968	1.2320
2	2.0325	2.0430
3	1.4469	1.4446

In Table 5 it can be seen that the d_{space} parameter (obtained from the manual analysis of the SAD pattern) does not correspond fully with the d parameter (obtained from the ICDD database), there is a slight difference from the two data of *d*. However, all d_{space} values are in the range of the ICDD database values. Table 5 shows that d_{space} corresponds to the ICDD data which has the *hkl* value indicating the FCC structured crystal field. The lattice constant value obtained from the AgNWs-PG sample calculation is 4.189 Å whereas in theory the lattice constant value is 4.082 Å [9]. After the d_{space} value is obtained as shown in Table 5, a manual calculation is performed using Microsoft Excel to prove that the d_{space} value corresponds to the *hkl* value formed in the XRD results using Eq. 2 with the results as in Table 6.

Table 6. Analysis of *hkl* values of AgNWs-PG

d_{space} (Å)	*h*	*k*	*l*	d_{space} theory	α	$\sqrt{h^2+k^2+l^2}$
2.0325	2	0	0	2.0410	4.082	2
2.0325	0	2	0	2.0410	4.082	2
2.0325	0	0	2	2.0410	4.082	2
1.4469	2	2	2	1.1784	4.082	3.4641
1.4469	2	2	0	1.4434	4.082	2.8284
1.4469	2	0	2	1.4434	4.082	2.8284
1.4469	0	2	2	1.4434	4.082	2.8284
1.3513	1	1	1	2.3568	4.082	1.7320
1.2968	3	1	1	1.2319	4.082	3.3166
1.2968	1	3	1	1.2319	4.082	3.3166
1.2968	1	1	3	1.2319	4.082	3.3166
1.3513	4	2	0	0.9137	4.082	4.4721
1.2968	4	2	2	0.8342	4.082	4.8989
1.9067	4	4	4	0.5897	4.082	6.9282

Table 6 shows that the hkl values analyzed manually using Eq. 2 indicate that the d_{space} values generated from the study do not fully correspond to the values from the calculation of d_{space}. However, the value is in the range of the d_{space} value calculated, so that it can be indicated that the hkl fields (220), (200), and (311) that are formed correspond to, whereas the other fields of hkl are not suitable because the values between the research and calculation of dspace have a very wide range.

The results of the study revealed that the results of the characterization performed are interconnected. The XRD characterization results indicated that both samples were crystal-indexed. This is supported by the SAD pattern data that shows crystallized SAD patterns characterized by the presence of spot–spot patterns, where each spot is related to specific atomic distances. The XRD results also showed that the two samples had five diffraction peaks related to the confirmed hkl values from the SAD pattern data calculated using Eq. 2, which had a hkl value corresponding to the resulting crystal structure was FCC. From the XRD results also used to measure FWHM to calculate the size of the crystal that affects the size of AgNWs.

The smaller the particle size of the XRD data, the smaller the diameter of the AgNWs; moreover, the greater the particle size, the larger the resulting diameter. This is confirmed by the TEM data, which shows that the size of AgNWs-EG, which is ~84 and ~133 nm, is smaller than that of AgNWs-PG, which is ~85 and ~264 nm. The size of the AgNWs also influences the peak absorption of AgNWs. The smaller the diameter of the AgNWs, the lower the peak; moreover, the larger the diameter of the AgNWs, the higher the peak. This peak of absorption is related to surface plasmon resonance (SPR). The wavelength of the maximum SPR is indicated by the influence of Ag particle size [24-26].

From the size of the AgNWs produced, this research can be used in making TCEs for optoelectronic applications. One application that has been successfully developed is the manufacture of thin films based on the AgNWs with the methods of dip coating and spray coating [14, 15, 21].

Summary

The formation of AgNWs generally consists of three stages: reduction, nucleation, and growth. The formation of AgNWs using PG solvents is faster than that using EG. The XRD characterization results indicated that both samples were crystal-indexed. This is supported by the SAD pattern data that shows crystallized SAD patterns characterized by the presence of spot–spot patterns, where each spot is related to specific atomic distances. The two crystallines diffracted indexed samples with the crystal structure formed are FCC, comprising five peaks with lattice fields (111), (200), (220), (311), and (222), respectively, by the lattice constant is 4.189 Å. The smaller the particle size of the XRD data, the smaller the diameter of the AgNWs; moreover, the greater the particle size, the larger the resulting diameter. The developed AgNWs can be used in making thin films for TCEs on optoelectronic devices.

Acknowledgment

This work was supported by a research grant of Professorship, Contract No. 1516/UN26.21/PN/2020 by Ministry of Research, Technology and Higher Education of the Republic of Indonesia via Institute for Research and Community Services of Universitas Lampung. The authors would like to thank Enago (www.enago.com) for the English language proofread and review.

References

[1] S. Coskun, B. Aksoy and H.E. Unalan, Polyol synthesis of silver nanowires: an extensive parametric study, *Cryst. Growth Des.* 11(5) (2011) 4963–4969, https://doi.org/10.1021/cg200874g.

[2] W.H. Chung, S.H. Kim and H.S. Kim, Welding of silver nanowire networks via flash white light and UV-C irradiation for highly conductive and reliable transparent electrodes, *Scientific Reports 6* (2016) 1–11, doi: 10.1038/srep32086.

[3] Y. Li, S. Guo, H. Yang, Y. Chao, S. Jiang and C. Wang, One-step synthesis of ultra-long silver nanowires of over 100 μm and their application in flexible transparent conductive films, *RSC Advances 8*(15) (2018) 8057–8063, https://doi.org/10.1039/C7RA13683H.

[4] K. Liu, Y. Li, H. Zhang and Y. Liu, Synthesis of the polypyrrole encapsulated copper nanowires with excellent oxidation resistance and temporal stability, *Appl. Surf. Sci. 439* (2018) 226–231, https://doi.org/10.1016/j.apsusc.2018.01.020.

[5] Z. Teymouri, L. Naji and Z. Fakharan, The influences of polyol process parameters on the optoelectronic characteristics of AgNWs-based flexible electrodes and their application in ITO-free polymer solar cells, *Org. Electron. 62* (2018) 621–629, https://doi.org/10.1016/j.orgel.2018.06.039.

[6] N. Truong, X. Minh, Q.T. Anh, B. Thi, M. Thu, L.P. Dung and N.T. Son, Effects of synthesis conditions on the formation and morphology of silver nanowires, *Vietnam Journal of Science & Technology 56* (2018) 111–117, https://doi.org/10.15625/2525-2518/56/2A/12637.

[7] N.D. Guzman, M. Ramos and M.D. Balela, Improvements in the electroless deposition of Ag nanowires in hot ethylene glycol for resistive touchscreen device, *Mater. Res. Bull. 106* (2018) 446–454, https://doi.org/10.1016/j.materresbull.2018.06.030.

[8] P. Zhang, I. Wyman, J. Hu, S. Lin, Z. Zhong, Y. Tu, Z.Huang, and Y. Wei, Silver nanowires: synthesis technologies, growth mechanism and multifunctional applications, *Mater. Sci. Eng. C* 223 (2017) 1–23, https://doi.org/10.1016/j.mseb.2017.05.002.

[9] H.S. Lee, Y.W. Kim, J.E. Kim, S.W. Yoon, T.Y. Kim, J.S. Noh, and K.S Suh,. Synthesis of dimension-controlled silver nanowires for highly conductive and transparent nanowire films, *Acta Materialia* 83 (2015) 84–90, https://doi.org/10.1016/j.actamat.2014.09.042.

[10] Junaidi, M. Yunus, Harsojo, E.Suharyadi and K. Triyana, Effect of stirring rate on the synthesis silver nanowires using polyvinyl alcohol as a capping agent by polyol process, *Int. J. Adv. Sci. Eng. Inf. Technol.* 6(3) (2016) 365, http://dx.doi.org/10.18517/ijaseit.6.3.808.

[11] V. Pokropivny, I. Hussainova and S. Vlassov, Introduction to Nanomaterials and Nanotechnology, Tartu University Press (2007) 1–138, ISBN: 978–9949–11–741–3.

[12] Junaidi, K. Triyana, Harsojo and E. Suharyadi, Controlling shapes and sizes of synthesis silver nanowires by polyol method using polyvinyl alcohol and polyvinyl pyrrolidone, *Indian Journal of Science and Technology* 10 (27) (2017) 1–8, DOI: 10.17485/ijst/2017/v10i27/93895.

[13] C. Jia, P. Yang and A. Zhang, Glycerol and ethylene glycol co-mediated synthesis of uniform multiple crystalline silver nanowires, *Mater. Chem. Phys.* 143(2) (2014) 794–800, https://doi.org/10.1016/j.matchemphys.2013.10.015.

[14] R. Becker, F. Söderlind, B. Liedberg and P.O. Käll, Synthesis of silver nanowires in aqueous solutions, *Mater. Lett.* 64 (8) (2010) 956–958, https://doi.org/10.1016/j.matlet.2010.01.072.

[15] L.V. Allen, The Art Science and Technology of Pharmaceutical Compounding. American Pharmaceutical Association, Washington DC: American Pharmacists Association (2002) 304–310, ISBN 987-1-58212-110-9.

[16] C.A. Rowe-Taitt, J.P. Golden, M.J. Feldstein, J.J. Cras, K.E. Hoffman and F.S. Ligler, Array biosensor for detection of biohazards, Biosen. *Bioelectron* 14(10-11) (2002) 785–794, https://doi.org/10.1016/S0956-5663(99)00052-4.

[17] M.B. Gebeyehu, T.F. Chala, S.Y. Chang, C.M. Wu and J.Y. Lee, Synthesis and highly effective purification of silver nanowires to enhance transmittance at low sheet resistance with simple polyol and scalable selective precipitation method, *RSC Advances 7*(26) (2017) 16139–16148, https://doi.org/10.1039/C7RA00238F.

[18] S.A. Kazmi, S. Hameed and A. Azam, Synthesis and characterization of Ag nanowires: Improved performance in dye sensitized solar cells, *Perspectives in Science 8* (2016) 577–579, https://doi.org/10.1016/j.pisc.2016.06.025.

[19] H.S. Lee, Y. Kim, J.E. Kim, S.W. Yoon, T.Y. Kim, J.S. Noh and K.S. Suh, Synthesis of dimension-controlled silver nanowires for highly conductive and transparent nanowire films, *Acta Materialia 83* (2015) 84–90, https://doi.org/10.1016/j.actamat.2014.09.042.

[20] Irzaman, Y. Sudiana, M. Hikam, W. Loeksmanto and M. Barmawi, Analisis struktur kristal dan Full Width Half Maximum (FWHM) dengan Metode Rietveld (Studi Kasus: Kalsit ($CaCO_3$)), *Kontribusi Fisika Indonesia* 11(2) (2000) 41–48 (in Indonesian).

[21] B. Wiley, Y. Sun and Y. Xia, Polyol synthesis of silver nanostructures: Control of product morphology with Fe(II) or Fe(III) Species, *Langmuir* 21(18) (2005) 8077–8080, https://doi.org/10.1021/la050887i.

[22] J.J. De-Yoreo and P.G. Vekilov, Principles of Crystal Nucleation and Growth, Biomineralization: Mineralogical Society of America USA, (2002) 57-93.

[23] Y. Xia, Y. Xiong, B. Lim and S.E. Skrabalak, Shape-Controlled Synthesis of metal nanocrystals: simple chemistry meets complex physics, *Angew. Chem. Int. Ed. Engl.* 48(1) (2009) 60–103, doi: 10.1002/anie.200802248.

[24] S.D. Solomon, M. Bahadory, A.V. Jeyarajasingam, S.A. Rutkowski and C. Boritz, Synthesis and study of silver nanoparticles, *J. Chem. Educ.* 84(2) (2007) 322, https://doi.org/10.1021/ed084p322.

[25] Junaidi, K. Triyana, E. Suharyadi, Harsojo and L.Y.L. Wu, The Roles of polyvinyl alcohol (PVA) as the capping agent on the polyol method for synthesizing silver nanowires, *J. Nano Res.* 49 (2017) 174-180, https://doi.org/10.4028/www.scientific.net/JNanoR.49.174.

[26] Junaidi, K. Triyana, Harsojo and E. Suharyadi, High-Performance silver nanowire film on flexible substrate prepared by meyer-rod coating, *IOP Conf. Ser.: Mater. Sci. Eng.* 202 (2017) 012055, doi:10.1088/1757-899X/202/1/012055.

17% Overall Similarity

Top sources found in the following databases:

- 15% Internet database
- Crossref database
- 3% Submitted Works database
- 6% Publications database
- Crossref Posted Content database

TOP SOURCES

The sources with the highest number of matches within the submission. Overlapping sources will not be displayed.

1	scientific.net Internet	7%
2	repository.lppm.unila.ac.id Internet	3%
3	Junaidi, Nur Asriyani, Simon Sembiring, Posman Manurung, Sutopo Ha... Crossref	1%
4	Higher Education Commission Pakistan on 2012-10-20 Submitted works	1%
5	Junaidi, Kuwat Triyana, Edi Suharyadi, Harsojo, Linda Y.L. Wu. "The Ro... Crossref	<1%
6	researchgate.net Internet	<1%
7	dycotecmaterials.com Internet	<1%
8	text-id.123dok.com Internet	<1%

9	Junaidi, K Triyana, Harsojo, E Suharyadi. "High-Performance Silver Na... Crossref	<1%
10	Siegfried Rebsdat, Dieter Mayer. "Ethylene Glycol", Wiley, 2000 Crossref	<1%
11	insightsociety.org Internet	<1%
12	University of Birmingham on 2013-01-03 Submitted works	<1%
13	University of Hull on 2016-07-28 Submitted works	<1%
14	open.metu.edu.tr Internet	<1%
15	link.springer.com Internet	<1%
16	researchcommons.waikato.ac.nz Internet	<1%